Thin–Walled Structures 198 (2024) 111678

Contents lists available at ScienceDirect

Thin-Walled Structures

journal homepage: www.elsevier.com/locate/tws

Full length article

Thermal-mechanical coupling analysis of membrane surface failure of the air-supported membrane structure under fire considering weld seams

Yaning Zhang [a,b], Ying Sun [a,b,*], Qiming Zhu [a,b], Zhenggang Cao [a,b], Yang Yu [a,b]

[a] Key Lab of Structures Dynamic Behavior and Control of the Ministry of Education, Harbin Institute of Technology, Harbin 150090, China
[b] Key Lab of Smart Prevention and Mitigation of Civil Engineering Disasters of the Ministry of Industry and Information Technology, Harbin Institute of Technology, Harbin 150090, China

ARTICLE INFO

Keywords:
Air-supported membrane structures
The full-scale fire test case
Thermal-mechanical coupling analysis
Membrane surface failure
Weld seams

ABSTRACT

The membrane surface failure by developing a tear in air-supported membrane structures under fire conditions affects the deflation and collapse of the structure. However, in most existing studies, the failure is evaluated only according to whether the membrane surface temperature reaches the burn-through temperature of the membrane materials, without considering the effect of internal pressure variation caused by fire, and there have been even few studies on the impact of weld seams on membrane surface. This paper introduces the simplified constitutive models for PVC membranes and weld seams and a numerical simulation method to analyze the stress on the membrane surface of air-supported membrane structures during fire, taking into consideration the coupling effect of high temperature and internal pressure change. Numerical responses and the results of the full-scale fire test case by HIT (Harbin Institute of Technology) team are compared to demonstrate the effectiveness and applicability of the proposed material models and the simulation method. The study shows that the weld seams are the weak parts of the membrane surface under fire. The membrane surface failure may not first occur at the maximum temperature point of the membrane surface and the initial failure temperature is much less than the burn-through temperature of the membrane materials. Moreover, the initial failure of membrane surface should be attributed to the coevolutionary results of the stress field on the membrane surface and the degraded material properties at elevated temperatures. If the temperature is the only index to determine membrane surface failure in the air-supported membrane structure under fire, the common reference failure temperature should be reduced (approximately 120 ℃ for weld seams and 140 ℃ for membranes). The present study is valuable for fire risk assessment, performance-based fire protection design, and coupled analysis of fire and wind disasters in membrane structures.

1. Introduction

The air-supported membrane structure is the construction in which pressurized air stiffens a flexible membrane material to form a certain stable shape and bearing capacity [1]. Due to its excellent structural characteristics, e.g., low cost, convenient construction, low carbon and other advantages, it is widely used in sports, exhibitions, coal shed and military, etc. At present, the air-supported membrane structure has become a significant part of the world's space structure field [2]. However, compared with classical structures, the air-supported membrane structure is more vulnerable to fire. On one hand, the properties of membrane materials itself at high temperature make it insufficient in fire resistance and on the other hand, membrane surface failure by easily developing a tear under the additional load caused by the fire generally is more prone to cause the structural deflation and collapse. Therefore, the analysis of membrane surface failure under fire conditions is crucial for fire risk assessment for air-supported membrane structures.

The most commonly used membrane materials for the air-supported membrane structure are PVC-coated woven fabrics. Many scholars have been investigated on their properties at high temperature. Chai et al. [3] conducted a series of combustion tests to study the burn-through properties of PVC membranes and found that the burn-through temperature was about 257 ℃. Zhang et al. [4] studied the combustion characteristics of some PVC membranes. The tests showed that the

* Corresponding author at: Key Lab of Structures Dynamic Behavior and Control of the Ministry of Education, Harbin Institute of Technology, Harbin 150090, China.
E-mail address: sunnyhit@hit.edu.cn (Y. Sun).

https://doi.org/10.1016/j.tws.2024.111678
Received 16 October 2023; Received in revised form 4 January 2024; Accepted 2 February 2024
Available online 3 February 2024

burn-through temperature was about 365.5 ℃–437.6 ℃. In other studies, Ma [5] carried out uniaxial tensile tests of PVC membranes and found that the stress-strain curves at different temperatures showed typical nonlinear characteristics. Yu et al. [6] also invetigated the mechanical properties of four types of PVC membranes at high-temperature by uniaxial tensile tests. The high-temperature test showed that the maximum tensile strength at 170 ℃ reduced to 57 %–59 % of that at 20 ℃ and the stress-strain curves of different types of PVC membranes had similar variations at high-temperature. Xue et al. [7] studied the mechanical properties of PVC membranes and weld seams at high-temperature through uniaxial tensile tests and concluded that the degradation of the weld seam strength was greater than that of the membrane and it was more sensitive to the temperature change. The weld seam loses the bearing capacity completely when the temperature is higher than 130 ℃ while the strength of membrane only decreases 21.3 %. Together, these studies indicate that the burn-through temperatures of the membrane materials are not consistent with the critical temperature at which mechanical properties are lost. Compared with traditional building materials such as concrete and steel, the bearing capacity of membrane materials at high temperature is very low which directly results in the membrane surface failure easily occurring in the event of fire.

When the membrane surface failure occurs during fire, the structural performance will be adversely affected which increases the fire risk for the air-supported membrane structure. Some scholars studied the structural performance by fire tests of the air-supported membrane structure. Hopkinson [8] carried out fire tests on the ellipse-planed structure (19 m × 9 m). The tests showed that the membrane surface failure initially resulted in a vertical slit and quickly expanded in the small fire tests, and the flame directly penetrated the hole on the membrane surface and the size of the final hole resembled the area of the flame in the large fire test. And he also found that the larger the air leakage area caused by membrane surface failure, the faster the structure collapsed. Custer [9] conducted the fire test on the irregular planed structure (6 m × 6 m) and found that at 10.5 min after the ignition, the membrane surface above the fire source failed by developing a tear nearly 0.9 m long and the tear rapidly extended to a length of 4.6 m. The entire structure collapsed before the backup fan could be used to hold it up. The Swedish National Testing Institute [10] also performed some fire tests on an air-supported membrane structure. The tests results showed that the membrane surface failure occurred at the weld seams. The full-scale fire test of the rectangular-planed air-supported membrane structure (38 m × 20 m) was carried out by Yu et al. [11] and he found that membrane surface failure under fire included two modes: the failure induced by high-temperature and internal pressure coupling and the failure induced by high-temperature. The first mode usually corresponds to the initial failure of the membrane surface and the second mode mainly occurs when the deflation causes the internal pressure to drop to such a low level that the membrane surface almost loses stress. The time interval between the two modes of failure was about 160 s in the destructive fire test. In view of all tests that has been mentioned so far, the initial failure of membrane surface under fire is caused by high temperature and internal pressure, and it can extremely accelerate the structural deflation and collapse. Therefore, it is more accurate to study the membrane surface failure under fire from the perspective of force analysis.

Most of the above test studies occurred in the last century and the test data are relatively rare. In recent years, with the advancement of computer technology, numerical simulation is becoming the main research approach for fire resistance of building structures. In terms of additional loads caused by fire for air-supported membrane structures, there has been many studies on the temperature field and the internal pressure change. These studies [12–16] have shown that the temperature field of the membrane surface is non-uniform and changes with time under fire and the area where the maximum heat flow is received appears approximately above the fire source. The internal pressure rises rapidly to the maximum value gradually going down and then levels off after the ignition and the maximum value may be several times greater than the working pressure [17]. However, in most existing studies on the membrane surface failure [18–23], the failure is evaluated only according to whether the membrane surface temperature reaches the burn-through temperature of the membrane materials. Only a few scholars analyzed the membrane surface failure from the perspective of thermal-mechanical coupling. Wang [24] investigated the stresses on the membrane surface under fire by ANSYS software. Yan et al. [25] analyzed the membrane surface failure for the perspective of safety coefficient. In Wang and Yan's studies, the linear constitutive model at different temperatures which is only for a certain PVC membrane material was applied. Unfortunately, internal pressure variation caused by fire was not taken into account and the failure mechanism of the membrane surface has not been studied in depth.

To sum up, the fire process of the air-supported membrane structure has the unique characteristics, e.g., non-uniform and time-varying temperature field, time-varying internal pressure, time-varying properties of components. In addition, PVC membrane is a typical nonlinear material and the mechanical properties of different materials at high temperature are different, but the previous material constitutive model considering the effect of the high temperature is only applicable to a single material or not universal. Moreover, the actual air-supported membrane structures are often made of pieces of membranes and usually there are some weld seams areas on the membrane surface. The above series of problems makes the membrane surface failure more complicated under fire. So far, there is no comprehensive study of membrane surface failure under fire conditions. Therefore, to better guide the performance-based fire protection design of the air-supported membrane structure, it is quite necessary to establish a general constitutive model and a relatively precise and systematic numerical simulation method to analyze the stress state and failure mechanism of the membrane surface during fire.

In this paper, the general simplified nonlinear constitutive models of PVC membranes and weld seams considering temperature effects are firstly proposed based on the high temperature test data of PVC fabric membrane materials in the open literature [5–7,26–31], which is suitable for any kind of PVC membrane materials, and then a thermal-mechanical coupling study of the membrane surface failure is carried out through the developed hybrid FDS-ABAQUS simulation approach, specifically for the fire test case of full-scale air-supported membrane structure previously conducted by HIT team [11]. In order to considering the aforementioned fire characteristics of the air-supported membrane structure in the analysis, subroutine VUMAT is written to apply the constitutive model in terms of time-varying membrane component properties, and the PYTHON script interface is built to import non-uniform and time-varying temperature field of the membrane surface into ABAQUS as the thermal boundary conditions, and the internal pressure variation is loaded using the fluid cavity module. The following effort is to perform some parametric analyzes. Finally, the section of conclusions and prospects are presented.

2. The general simplified nonlinear constitutive models

As reviewed [5–7,26–31], the available high-temperature mechanical properties data of PVC membranes and weld seams in the existing literatures was collected. Drawing on the high-temperature material models in steel structure fire resistance studies [32], the effect of temperature on the mechanical parameters of different membrane materials is expressed by the dimensionless temperature influence coefficients and the polynomial regressive analyzes are employed to obtain the best fits for the statistical law of the overall data. Due to the relatively large

sample size of materials, the fitted laws can be well applied to any other PVC membrane material to a certain degree. This enriches the means of acquiring the high temperature mechanical parameters of membrane materials in fire resistance analysis for air-supported membrane structures.

PVC membrane materials are typical orthotropic materials and their elastic constitutive models at different temperatures established are as follows [33,34]

$$\begin{bmatrix} d\sigma_w \\ d\sigma_f \\ d\tau_{wf} \end{bmatrix} = \begin{bmatrix} \frac{E_w(T)}{1-\upsilon_{wf}(T)\upsilon_{fw}(T)} & \frac{\upsilon_{fw}(T)\cdot E_f(T)}{1-\upsilon_{wf}(T)\upsilon_{fw}(T)} & 0 \\ \frac{\upsilon_{wf}(T)\cdot E_w(T)}{1-\upsilon_{wf}(T)\upsilon_{fw}(T)} & \frac{E_f(T)}{1-\upsilon_{wf}(T)\upsilon_{fw}(T)} & 0 \\ 0 & 0 & G_{wf}(T) \end{bmatrix} \cdot \begin{bmatrix} d\varepsilon_w - d\varepsilon_w^T \\ d\varepsilon_f - d\varepsilon_f^T \\ d\gamma_{wf} - d\gamma_{wf}^T \end{bmatrix} \tag{1}$$

$$\begin{bmatrix} d\varepsilon_w^T \\ d\varepsilon_f^T \\ d\gamma_{wf}^T \end{bmatrix} = \begin{bmatrix} \alpha_w(T)\alpha_f(T)0 \end{bmatrix} \cdot \begin{bmatrix} \Delta T \\ \Delta T \\ 0 \end{bmatrix} \tag{2}$$

$$\sigma(T) = \begin{cases} \sigma(T) \le \alpha\cdot UTS(T)\ldots \\ E_{\mathrm{I}}(T)\cdot\varepsilon(T) \\ \alpha\cdot UTS(T) \le \sigma(T) \le \beta\cdot UTS(T)\ldots \\ E_{\mathrm{II}}(T)\cdot\varepsilon(T) + \dfrac{\alpha(E_{\mathrm{I}}(T) - E_{\mathrm{II}}(T))\cdot UTS(T)}{E_{\mathrm{I}}(T)} \\ \beta\cdot UTS(T) \le \sigma(T) \le UTS(T)\ldots \\ E_{\mathrm{III}}(T)\cdot\varepsilon(T) + \dfrac{(\beta\cdot E_{\mathrm{I}}(T)\cdot E_{\mathrm{II}}(T) - (\beta-\alpha)E_{\mathrm{I}}(T)\cdot E_{\mathrm{III}}(T) - \alpha\cdot E_{\mathrm{II}}(T)\cdot E_{\mathrm{III}}(T))\cdot UTS(T)}{E_{\mathrm{I}}(T)\cdot E_{\mathrm{II}}(T)} \end{cases} \tag{3}$$

Where E_w,E_f denote tensile modulus in the warp and weft directions respectively. G_{wf} denotes the shearing modulus. υ_{wf},υ_{fw} denote the Poisson's ratio in the warp and weft directions respectively. α_w,α_f denote coefficient of thermal expansions in the warp and weft directions respectively. Poisson's ratio and thermal expansion coefficient may show temperature correlation and stress correlation [35], but due to the lack of relevant research, they are treated as constants and G_{wf} is taken as 1/20 of the tensile modulus in the warp direction in this paper [36,37].

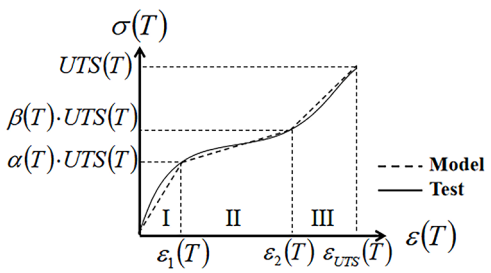

Fig. 1. The reformulated three-segment model of PVC membranes.

2.1. Constitutive parameters for PVC membranes

The simple way to describe the nonlinearity of the stress-strain curve of the material is to use a piecewise linear function, and the elastic constant can be approximated by a multi-step linear method for more accurate material nonlinearity analysis [38]. Studies [5–7,26–31] have shown that the uniaxial tensile stress-strain curve of PVC membranes at different temperatures can be illustrated to the three-segment model: the initial linear segment, the strain-reinforced segment and the stress-reinforced segment. However, a general mathematical expression for this model has not been established because of the little regularity for the model division points from the strain perspective. For this purpose, the three-segments model is reformulated in Fig. 1, where the previous division points are replaced by re-established division points from the stress perspective. Here, *UTS* is the ultimate tensile strength, ε_{UTS} is the strain corresponding to the ultimate tensile strength, ε_{I} and $\varepsilon_{\mathrm{II}}$ are the strain division points used in the current studies, $\alpha\cdot UTS$and $\beta\cdot UTS$are the re-established stress division points corresponding to ε_{I} and $\varepsilon_{\mathrm{II}}$, respectively, and E_{I}, E_{II} and E_{III}denote the tensile modulus of the three segments, respectively. So the mathematical expression of the model can be illustrated as Eq. (3).

The dimensionless temperature influence coefficients of the parameters in the model are defined as Eqs. (4)–(6). Based on the data collected [5–7,26–31], the statistical laws of the above dimensionless coefficients are presented by polynomial fitting in Figs. 2–4 and Eqs. (7)–(13). It can be seen in Fig. 2 that TIC_{UTS} of different PVC membranes has strong regularity. Therefore, compared with previous strain division points, the regularities of re-established stress division points can be better indirectly expressed by TIC_{UTS}. As shown in Fig. 3, the stress division points exhibit significant differences between different materials or between the warp and weft directions of the same materials. In contrast, the differences of the stress division points between different temperatures for the same materials are small. Consequently, the constant value is used for the stress division points for the same kind of PVC membrane in general mathematical expression of the model for further simplification to facilitate application.

Up to this point, once the tensile stress-strain curve of any PVC membranes at room temperature is procured, its tensile properties at any high temperature can be predicted appropriately according to the established statistical laws.

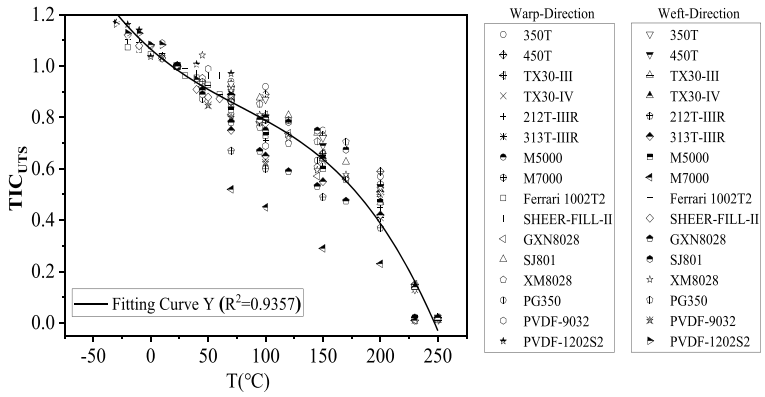

Fig. 2. TIC_{UTS} of PVC membranes.

Ultimate tensile strength :

$$TIC_{UTS} = UTS(T)/UTS(20^{\circ}C) \tag{4}$$

Stress division points :

$$TIC_{\alpha} = \alpha(T)\cdot UTS(T)/UTS(T)$$
$$TIC_{\beta} = \beta(T)\cdot UTS(T)/UTS(T) \tag{5}$$

Tensile modulus :

$$TIC_{E} = E(T)/E(20^{\circ}C) \tag{6}$$

$$TIC_{UTS}(T) = 1.0663 - 0.0040\times T + \left(2.0875\times 10^{-5}\right)\times T^{2} - \left(9.0315\times 10^{-8}\right)\times T^{3} \tag{7}$$

Warp:

$$TIC_{E_{\mathrm{I}}}(T) = 1.1268 - 0.0062\times T + \left(2.1197\times 10^{-5}\right)\times T^{2} - \left(4.1327\times 10^{-8}\right)\times T^{3} \tag{8}$$

$$TIC_{E_{\mathrm{II}}}(T) = 1.1148 - 0.0048\times T + \left(1.7640\times 10^{-5}\right)\times T^{2} - \left(4.6556\times 10^{-8}\right)\times T^{3} \tag{9}$$

$$TIC_{E_{\mathrm{III}}}(T) = 0.9817 + 0.0009\times T - \left(7.0327\times 10^{-5}\right)\times T^{2} + \left(2.8962\times 10^{-7}\right)\times T^{3} \tag{10}$$

Weft :

$$TIC_{E_{\mathrm{I}}}(T) = 1.2963 - 0.0153\times T + \left(1.3744\times 10^{-4}\right)\times T^{2} - \left(4.5090\times 10^{-7}\right)\times T^{3} \tag{11}$$

$$TIC_{E_{\mathrm{II}}}(T) = 1.1222 - 0.0047\times T + \left(8.2739\times 10^{-6}\right)\times T^{2} + \left(7.6986\times 10^{-9}\right)\times T^{3} \tag{12}$$

$$TIC_{E_{\mathrm{III}}}(T) = 1.0064 + 0.0016\times T - \left(7.7875\times 10^{-5}\right)\times T^{2} + \left(2.8586\times 10^{-7}\right)\times T^{3} \tag{13}$$

In addition, the shearing strength S is determined by the Eq. (13) [39]:

$$S = \frac{0.8UTS_{45^{\circ}}}{\sqrt{2}} \tag{14}$$

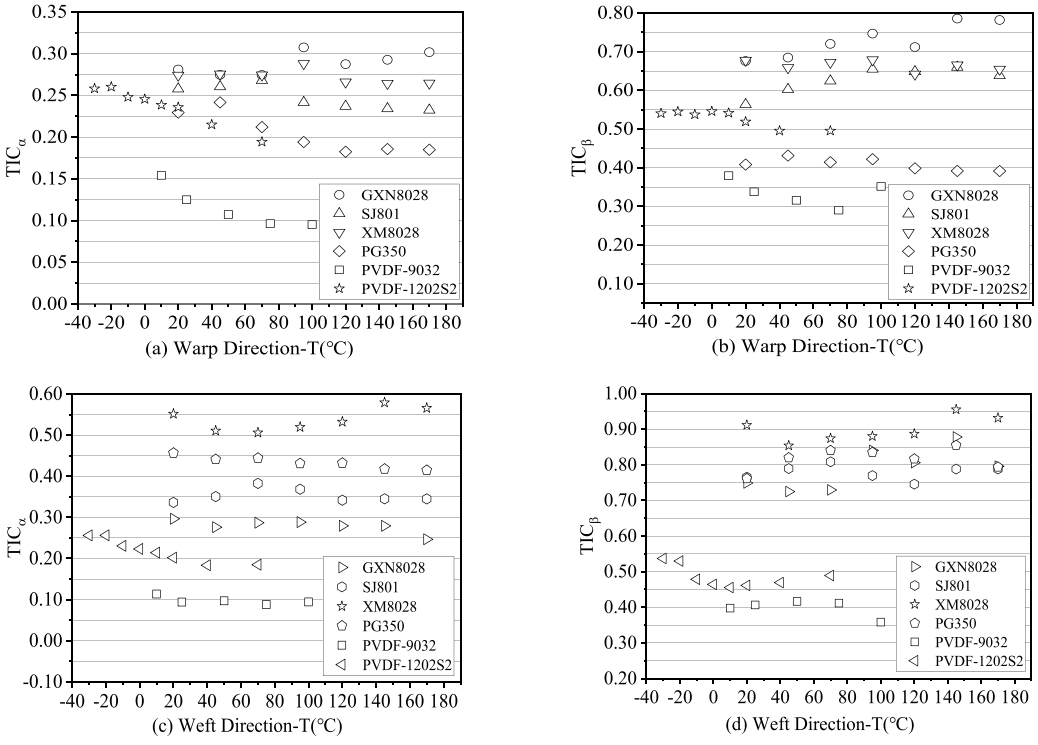

Fig. 3. Stress division points of PVC membranes.

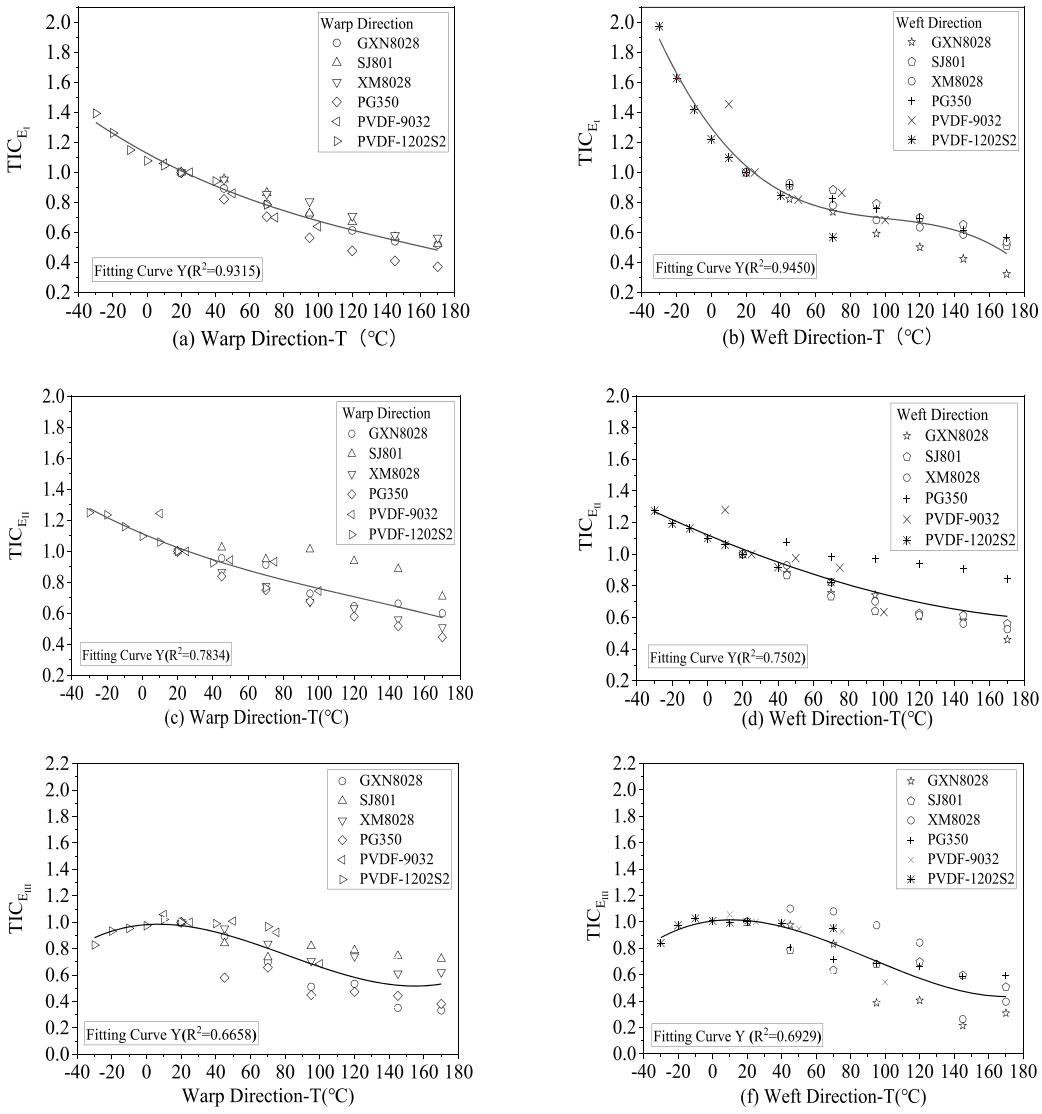

Fig. 4. TIC_E of PVC membranes.

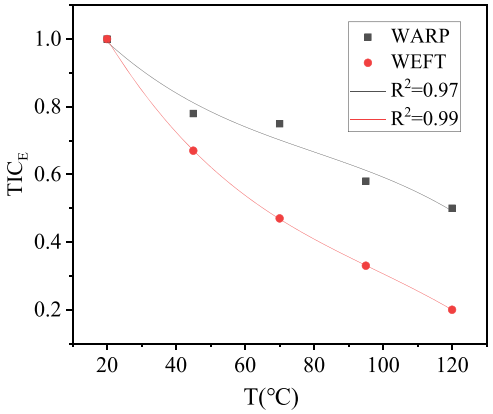

Fig. 5. TIC_E of weld seams.

where the off-axis ultimate tensile strength $UTS_{45°}$ is approximated as half of the ultimate tensile strength in the warp direction [40].

2.2. Constitutive parameters for weld seams

Due to the effect of the curvature of the building shape, there are usually weld seams on the membrane surface of the air-supported membrane structure. This section analyzes the weld seams where the membrane is connected parallel to the warp or weft direction. For example, weld seams in the span direction of structures are generally weft parallel connection forms, whose mechanical properties in the warp direction are same as those of membranes. Vertical connection forms of weld seams do not get attention here. On the one hand, there are few researches on the their mechanical properties. On the other hand, such weld seams are usually situated at the corner of air-supported membrane structures [41] and are distant from the location of membrane surface failure in full-scale fire test case, which has minimal impact on the force of the failure location according to Saint-Venant principle [42].

Based on the data in literatures [7,43], a linear elastic model of uniaxial tensile stress-strain curve is used here. TIC_E is presented in Fig. 5 and Eqs. (15) and (16). TIC_{UTS} directly adopts the average results in above both literatures, as presented in Eq. (17).

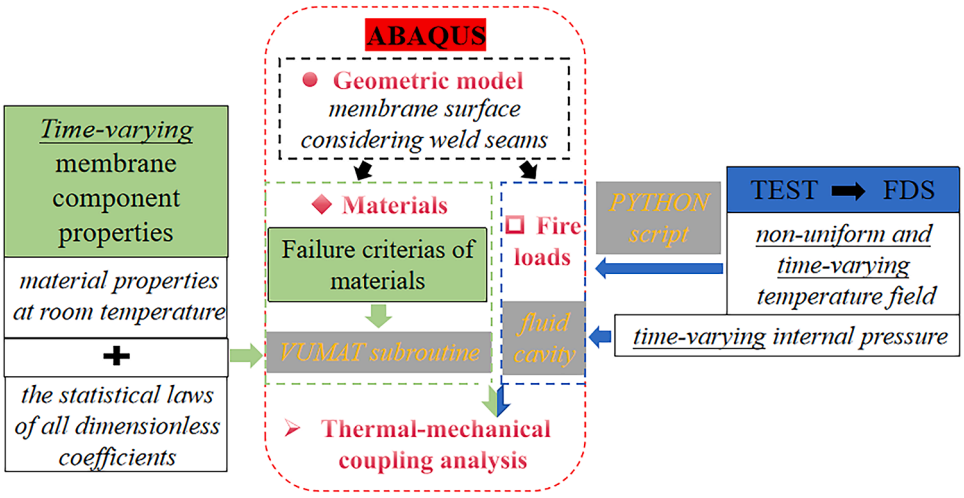

Fig. 6. The analysis flow chart.

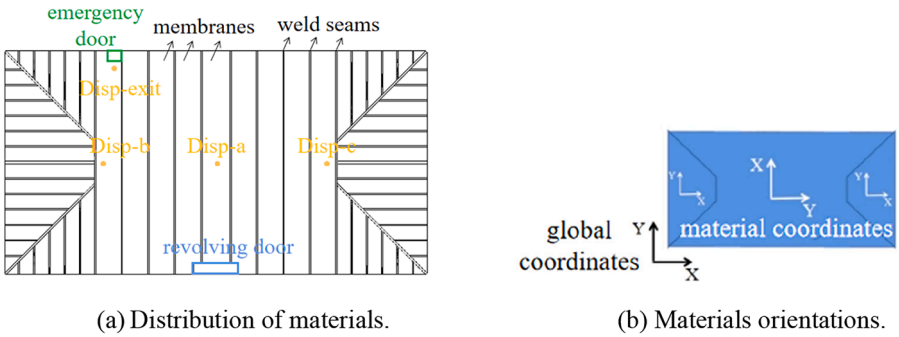

(a) Distribution of materials. (b) Materials orientations.

Fig. 7. Membrane surface information.

$$Warp: TIC_E = 1.22 - 0.0138 \times T + \left(1.28 \times 10^{-4}\right) \times T^2 - \left(5.33 \times 10^{-7}\right) \times T^3 \quad (15)$$

$$Weft: TIC_E = 1.39 - 0.0232 \times T + \left(1.87 \times 10^{-4}\right) \times T^2 - \left(6.40 \times 10^{-7}\right) \times T^3 \quad (16)$$

$$TIC_{UTS} = -0.0091 \times \mathrm{T} + 1.182 \quad (17)$$

3. Thermal-mechanical coupling analysis of membrane surface failure considering weld seams

In the full-scale fire test case [11], the rectangular-planed air--supported membrane structure measured 38 m x 20 m and was 7 m high at the apex. The air volume enclosed in envelope was approximately 4573 m^3. The inflation system consisted of two fans, with a maximum air inlet capacity of 23,000 m^3/h. The fan was equipped with pressure sensors to adjust the air intake according to the internal pressure. The working pressure of air-supported membrane structure was around 200 Pa. The fire source was located in the center of the structure, with the shape of a circle and the diameter of 1.5 m. The fuel adopted the n-heptane. The fitting curve of the fire power in the test remained relatively horizontal after linearly rising to the maximum power of 3200 KW in 73 s.

The concept of thermodynamic coupling generally is focused on the interaction between the stress field and the temperature field [44], but in this section the emphasis is placed on the comparison between the joint action of temperature and stress and the single action. The sequential thermal-mechanical coupling method where the fire-induced loads solved by FDS software are imported into ABAQUS platform is used. It is essentially a one-way coupling of the temperature field to the stress field [45]. Furthermore, it is approximated as a quasi-static process before structural collapse under fire conditions [46]. Each loading step of the quasi-static state is calculated independently according to the constraints and loads of this step based on the initial configuration of the structure [37,47]. The flow chart of the quasi-static analysis of thermal-mechanical coupling of membrane surface failure developed in this paper is shown in Fig. 6. In ABAQUS, the membrane surface uses M3D3 element and the fluid element is F3D3. Mesh density selection coordinates precision, convergence and computation time, totaling 28, 752 cells in the present work. On account of the nonlinearity of the membrane material itself, the degradation of membrane performance caused by the fire, and the geometric nonlinearity resulting from large deformation [48], the explicit scheme is adopted here.

Table 1
Values of material constitutive parameters (20 ℃).

	Warp (MPa)			Weft (MPa)			Warp (kN/m)	Weft (kN/m)	υ_{wf}	α
	E_I	E_{II}	E_{III}	E_I	E_{II}	E_{III}	UTS	UTS		
Mem-	214	92	168	105	80	230	80	66	0.4	0.0001
welds	214	92	168	161.3			80	66		

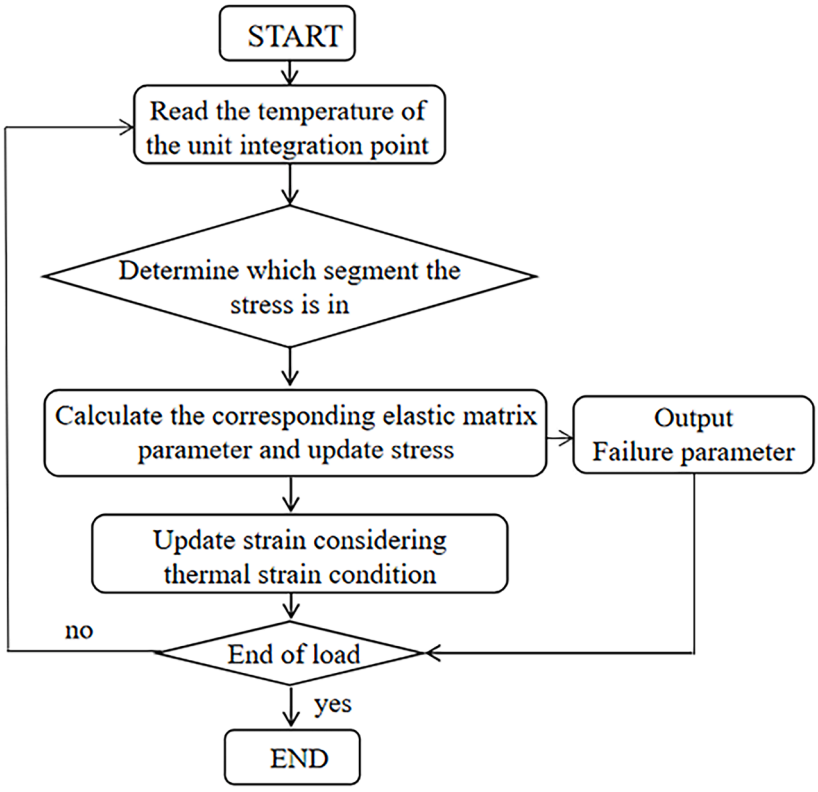

Fig. 8. The logic of code execution for VUMAT.

3.1. Membrane surface considering weld seams

In the design of the membrane structures, the membrane surface are usually composed of pieces of membranes which are connected by weld seams [49]. Studies [7] have shown that peel-off is the primary failure mode for weld seams under high temperature and there is a possibility of fracture occurring in the base material near the adjacent overlap area due to stress concentration. Therefore, the width of the weld seams is consistently set at 10 cm for the purpose of simulation taking into consideration the area of the overlap section along with both sides.

According to the information from full scale air-supported membrane structure in fire test case [11], based on form finding and cutting patterns [50], the geometric model of the structure was established by RHINO software. The distribution of the membranes and weld seams on the membrane surface is illustrated in Fig. 7 (a) where each membrane is about 2.5 m wide.

3.2. Materials

The constitutive parameters at room temperature of membranes and weld seams forming the envelope of the structure in the fire test are given in Table 1, and the density is 1300 kg/m^3. The constitutive parameters at elevated temperatures are obtained by the statistical laws in Section 2, where $\alpha = 0.12$ and $\beta = 0.33$ are taken at the warp division points and $\alpha = 0.10$ and $\beta = 0.40$ are taken at the weft division points for membranes. Materials orientation on the membrane surface is presented in Fig. 7 (b) where X represents the warp direction. The discrete coordinate system is used to define the directions of the materials in ABAQUS.

3.2.1. The time-varying properties

Explicit subroutine VUMAT is used to realize the time-varying properties of materials in the thermal-mechanical coupling analysis. Fig. 8 provides the logic of code execution for VUMAT.

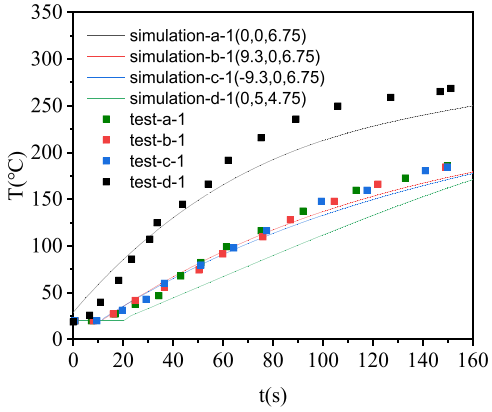

Fig. 9. Comparisions of spatial measurement points near the membrane surface.

3.2.2. Failure criterias

A few studies have indicated [40,51,52] that both the Tsai-Hill criterion and the Hashin criterion are applicable for predicting failure in PVC membranes under specific stress conditions. Both criterias belong to the scope of macroscopic strength theory, and do not involve the specific internal structure and failure form of the material [53]. Although there are differences between the weld seam and the membrane in the microscopic aspect, both are essentially orthotropic materials, so the same failure criteria are used in this paper. In addition, considering the complexity of membrane surface stress under fire, the above both criterias are adopted. The expressions for both criterias are as follows:

$$Tsai-Hill\ failure\ criterion:$$

$$\frac{\sigma_w(t)^2}{X(T)^2} - \frac{\sigma_w(t)\sigma_f(t)}{X(T)^2} + \frac{\sigma_f(t)^2}{Y(T)^2} + \frac{\tau_{wf}(t)^2}{S(T)^2} = 1 \tag{18}$$

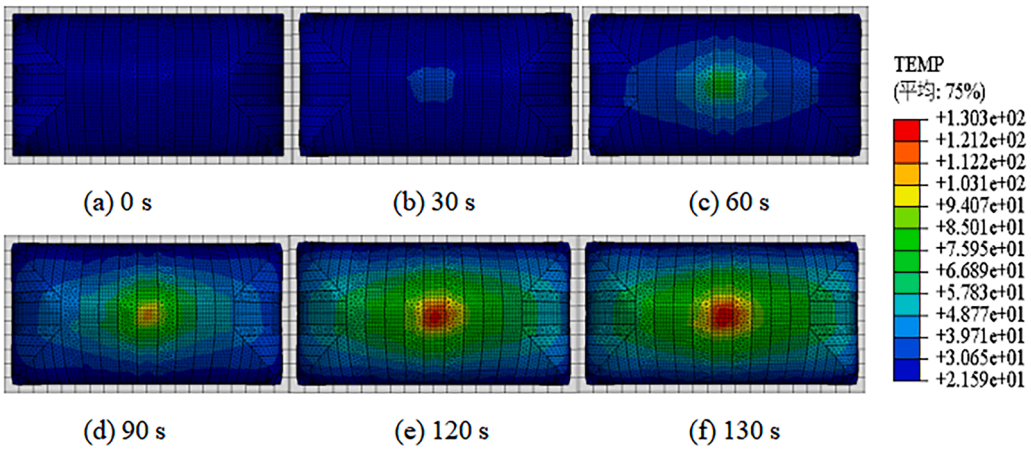

Fig. 10. Temperature field of the membrane surface (℃).

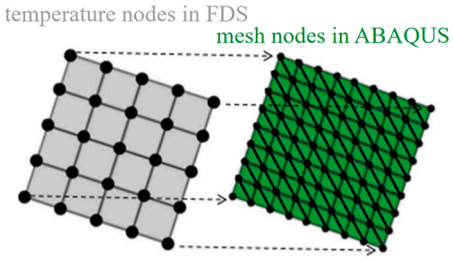

Fig. 11. Coordinate-based mapping model of temperature field on membrane surface.

Hashin warp tensile failure criterion :

$$\frac{\sigma_w(t)^2}{X(T)^2}+\frac{\tau_{wf}(t)^2}{S(T)^2}=1 \tag{19}$$

Hashin weft tensile failure criterion :

$$\frac{\sigma_f(t)^2}{Y(T)^2}+\frac{\tau_{wf}(t)^2}{S(T)^2}=1 \tag{20}$$

Where σ_w(t),σ_f(t) denote the normal stress in the warp and weft directions, respectively. τ_{wf}(t) denotes the shear stress. X(T), Y(T) and S(T) denote the ultimate uniaxial tensile strength in the warp and weft directions and the shearing strength, respectively.

In order to evaluate whether the membrane surface failure occurred during the fire in the simulation, the left half of the Tsai-Hill criterion and Hashin criterion are defined as the failure parameters. The result of these parameters is output by the state variables in VUMAT.

3.3. Fire-induced loads

On the basis of the fire test case, more detailed fire-induced loads data, mainly including the non-uniform and time-varying temperature field and internal pressure variation is obtained by the large eddy simulation method of FDS software.

3.3.1. Temperature field

For the heat dissipation of the membrane surface, it is mainly considered by setting the thermophysical characteristic of the membrane material and the thermal boundary conditions on both the inside and outside of the membrane surface. The themal conductivity is taken as $0.1W/(m{\cdot}K)$ and the specific heat capacity is taken as $1.0\ kJ/(kg{\cdot}K)$. The heat radiation and heat convection on the inner surface are determined automatically by FDS, and the heat transfer of the air near the inner and outer surface is calculated by BACKING parameters [54]. Since only the data of the spatial temperature measuring points is given in the test case, this paper uses these test results in comparison with the simulation results to determine the optimal simulation conditions, and then extracts more detailed temperature field results of the membrane surface for the thermal-mechanical coupling analysis.

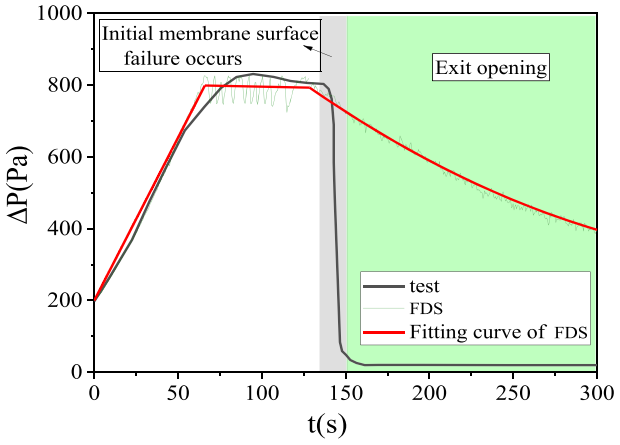

Fig. 12. Comparisons of internal pressure.

The time history results of the temperature of the four spatial measuring points near the membrane surface are compared in Fig. 9. In contrast, the large differences in detail can be seen between the curves because the simulation is simplified on the basis of the complexity of the actual test environment and combustion reaction, but overall, the numerically simulation results match reasonably test data.

In the thermal-mechanical coupling analysis of structural fire resistance, it is crucial to select the appropriate time step due to the fact that the evolution rate of air temperature near the member surface is always faster than the internal heat conduction rate of the member [55]. This issue is avoided in this study by directly extracting the temperature field on the membrane surface in FDS. As shown in Fig. 10, the temperature field data of the membrane surface obtained by post-processing subroutine fds2ascii shows the non-uniform and time-varying characteristics. The maximum temperature point on the membrane surface always appears directly above the fire source. It is worth noting that after the fire power reaches the maximum value at 73 s, the temperature of the membrane surface is still rising but the rate of rise gradually slows down.

Additionally, when the ratio of surface area to volume per unit length of the member (F/V) is greater than 300, the temperature distribution of the cross-section of the member is assumed to be uniform and equal to

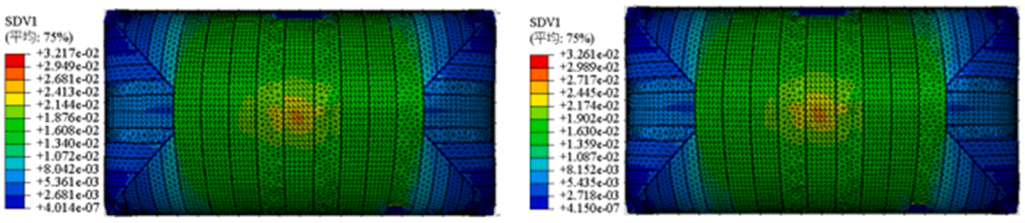

(a) Hashin tensile failure parameters in warp.

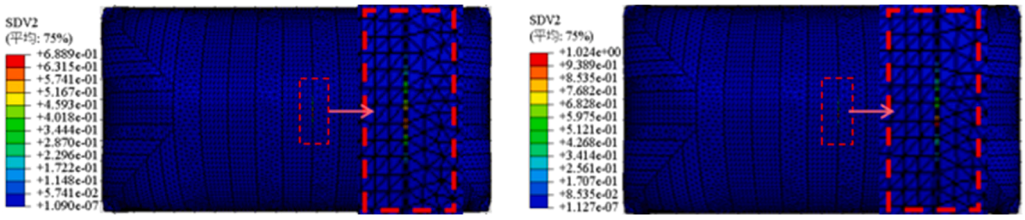

(b) Hashin tensile failure parameters in weft.

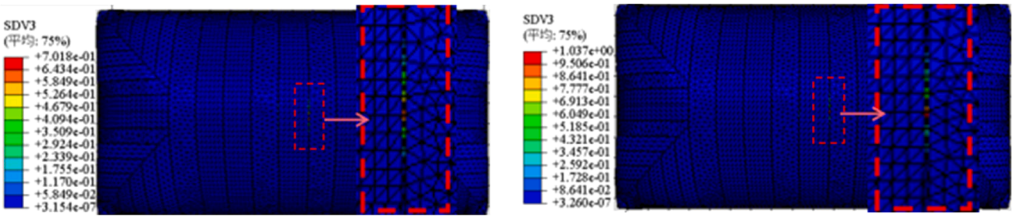

(c) Tsai-hill failure parameters.

Fig. 13. The analysis of membrane surface failure (the left is 126 s, the right is 127 s).

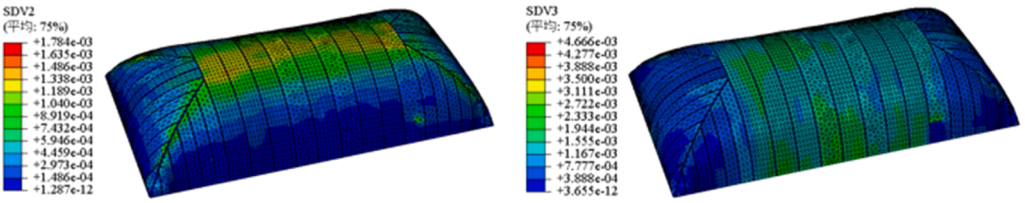

(a)10s

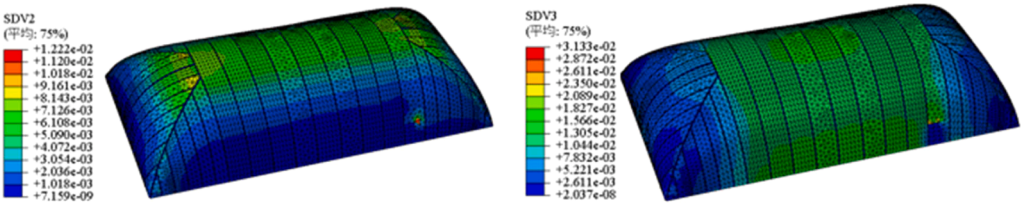

(b)70s

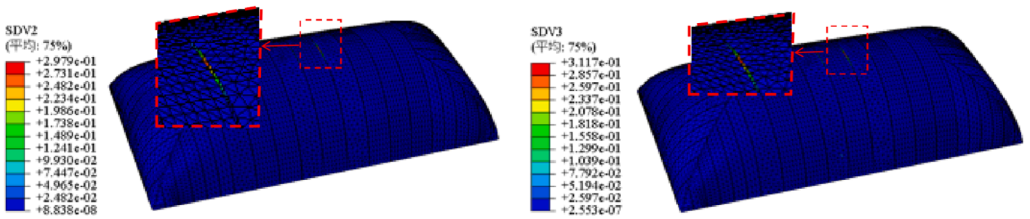

(c) 120s

Fig. 14. Failure parameters of Hashin in weft (left) and Tsai-hill (right) during fire.

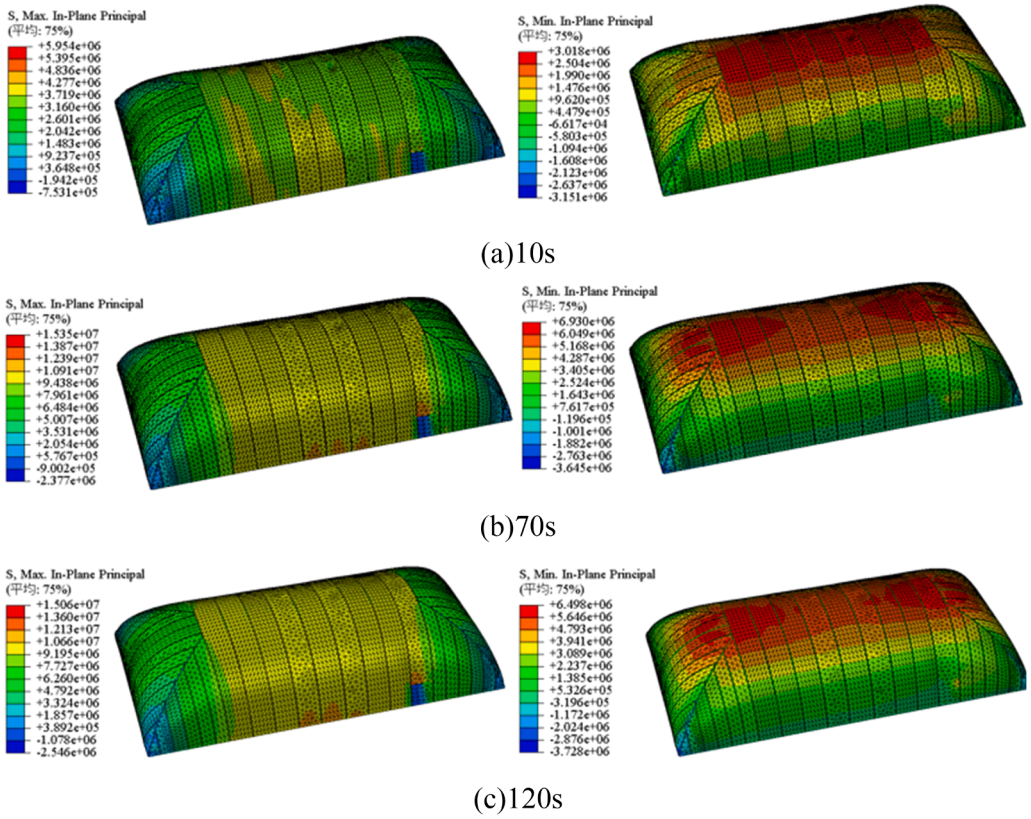

Fig. 15. Maximum principal stress (left) and minimum principal stress (right) during fire.

the temperature of the surface exposed to fire in the fire resistance analysis of steel structures [56]. Therefore, heat transfer analysis is not need to be conducted in the thermal-mechanical coupling analysis for membrane structures in ABAQUS.

The principle of the PYTHON script interface is shown in Fig. 11. The temperature field result on the membrane surface is imported to ABAQUS as the thermal boundary conditions mainly by the 3D (X, Y, and TEMPERATURE) inverse distance-weighted interpolation algorithm where the temperature field data (with a 10 s interval) is mapped to the ABAQUS computational grid nodes. This method has both efficiency and accuracy of data transfer [57].

3.3.2. *Internal pressure*

In actual air-supported membrane buildings, the normal air leakage occurs through some small gaps between membranes, by foundation or entrances and other conceivable leakage paths. Those induced equivalent air leakage area is taken as 0.28 m^2 in the test case [11,37]. Due to the characteristics of sub-grid scale leakage, normal air leakage is simulated by pressure zones and HVAC module in FDS which assumes that this type of leakage occurs in a specific designated leakage area connected to the outside through a very small pipe [17]. The fan is controlled by COMMAND statements. The conditions of membrane surface failure and the exit opening in the test case are not considered in this simulation. The internal pressure results are compared in Fig. 12. A close agreement is found between both curves before the initial membrane surface failure.

In ABAQUS, the direct pressure load method is applied at the boundary of the model, which may cause stress concentration and numerical instability at the weld seams of the membrane surface, while the fluid cavity method utilizes the fluid element to apply the pressure load, which can distribute the load more evenly and reduce stress concentration, as well as enhance numerical stability [58]. Therefore, the fitting result of internal pressure is loaded by the fluid cavity method in the thermal-mechanical coupling analysis.

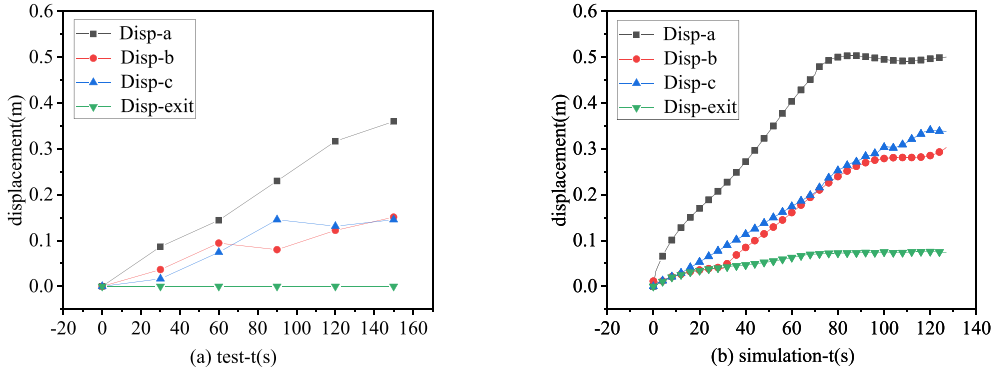

Fig. 16. Comparisons of displacement responses.

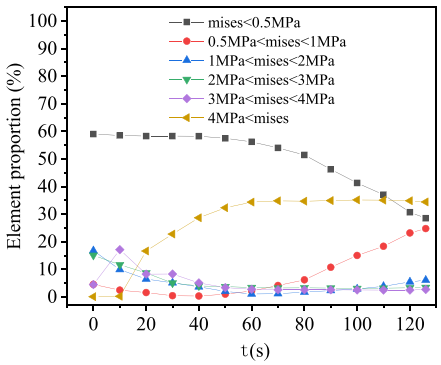

(a) Thermal-mechanical coupling.

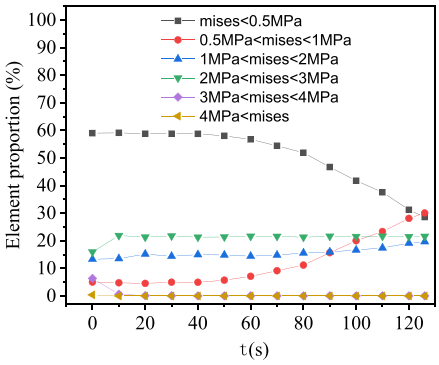

(b) Temperature field alone (200Pa).

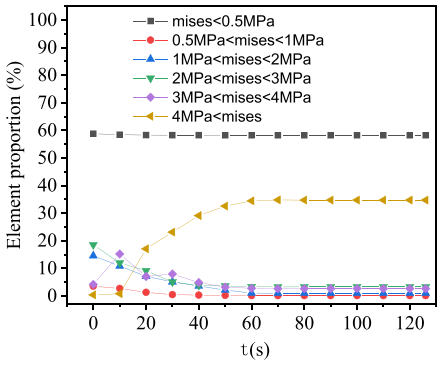

(c) Internal pressure alone (20 °C).

Fig. 17. Effect of temperature and internal pressure on mises stress variation.

3.4. Structural responses during fire

Structural responses in the full-scale fire test case and the corresponding numerical results including the membrane surface failure and displacement responses of measuring points on membrane surface are compared to demonstrate the effectiveness and applicability of the proposed material models and the simulation method. More detailed information not measured in the test is also analyzed.

3.4.1. Membrane surface failure

The membrane surface failure ocurred at the weld seams above the fire source at 135 s in the test case [11]. The result of Hashin and Tsai-hill failure parameters for predicting the membrane surface failure is presented in Fig. 13. From the graph it can be seen that both failure parameters show that the weld seams of the membrane surface is first failed at 127 s which is very close to the test results. This reflects that both Hashin criterion and Tsai-hill criterion can meet the analysis of membrane surface failure under fire. Besides, of interest here is that the area where the maximum heat flow is received on the membrane surface in Fig. 10 is not the position where the membrane surface failure first occurs, which confirms the limitation of most previous studies that only consider the temperature effect. The failure may not initially occur at the maximum temperature point of the membrane surface for the air-supported membrane structure under fire.

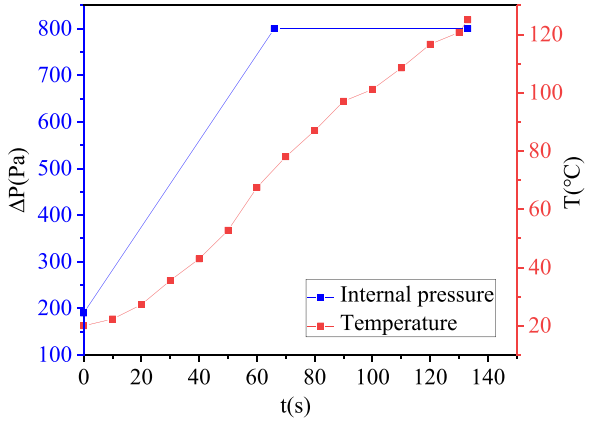

Fig. 18. Temperature and internal pressure acting on the failure element during fire.

As shown in Fig. 14, the results of membrane surface failure parameters during fire show that the maximum value of the Hashin tensile failure parameter in weft always occurs at the top membrane position along the long axis of the structure, while the maximum value of the Tsai-hill failure parameter consistently appears in the middle membrane position along the long axis of the structure. With the development of the fire, the distribution area of the maximum value gradually shrinks. This indicates that the most susceptible failure region of the air-supported membrane structure at normal working temperature probably is also the most vulnerable part during fire, only for cases where the fire is in the center of the structure. When the fire occurs in the corners or near the edges of the structure, the failure may be relatively different.

3.4.2. Stress redistribution of membrane surface

Although the strength of the PVC membrane materials is different in each direction, the direction of the principal stress may be not the most dangerous direction, but the principal stress is also analyzed in this section in order to better understand the stress state of the membrane surface.

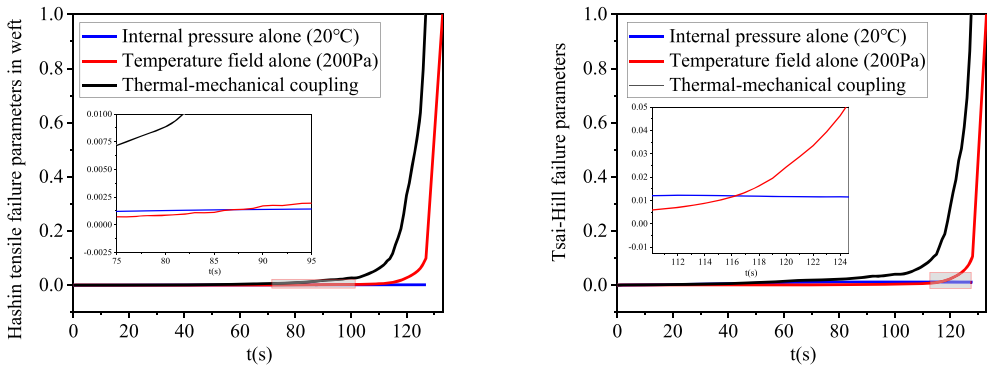

(a) Hashin tensile failure parameter in weft (b) Tsai-hill failure parameter

Fig. 19. Variation of failure parameters of failure element.

Table 2
Statistical information of the failure element.

	Temperature (℃)	Pressure (Pa)	Failure time (s)
Thermal-mechanical coupling	119	800	127
Temperature field alone	125	200	133
Internal pressure alone	20	800	/

The results of the maximum and minimum principal stresses of the membrane surface during fire in Fig. 15 suggest that the distribution of maximum stress or minimum stress has almost no significant change when the internal pressure remains almost constant after 70 s and the stress concentration is not obvious at the weld seams where the failure occurred. In general, the internal pressure has a more compelling effect on the stress redistribution of the membrane surface than the temperature.

3.4.3. *Displacement responses of measuring points on membrane surface*

The locations of four displacement measuring points are presented on the membrane surface in fire test case, as shown in Fig. 7 (a). Comparisons of displacement responses in Fig. 16 indicate that the displacement in the simulation is larger than in the test, exceeding 0.1-0.2 m. This difference is mainly due to simplification in the material constitutive. Compared with the analysis in Section 3.4.2, it can be found that the displacement of some areas of the membrane surface still increased 70 s after the fire although the principal stress did not change much.

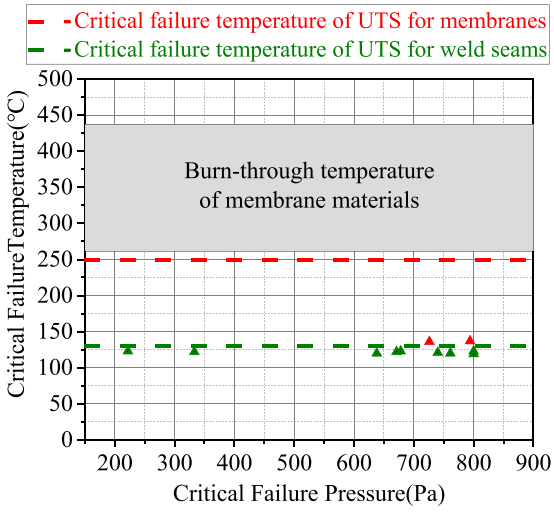

Fig. 20. Critical failure temperature and critical failure internal pressure of elements.

3.5. *Mechanism of membrane surface failure*

The contributions of temperature and internal pressure respectively to the membrane surface failure and their impacts on stress distribution during fire are analyzed by comparing the results of the three cases, including Case 1: thermal-mechanical coupling analysis, Case 2: the analysis of only considering time-varying temperature field alone where the internal pressure is maintained in normal working condition (200

Table 3
Working condition details and simulation results.

Fire source position	Height of the membrane surface above the fire source(m)	Max-power of fire (MW)	Type of fire growth	Initial failure position	Critical failure temperature (℃)	Critical failure pressure (Pa)	Failure Time by coupling (s)	Failure Time only by temperature-250 ℃ (s)
(0,0,0)	7	1	test	Weld seams	123	222	931	/
(0,0,0)	7	2	test	Weld seams	122	333	322	/
(0,0,0)	7	3.2	test	Weld seams	119	800	127	301
(0,0,0)	7	4	test	membranes	137	794	84	185
(0,-6,0)	4.75	3.2	test	membranes	136	726	60	84
(-12,0,0)	6.68	3.2	test	Weld seams	120	800	122	316
(-12,-6,0)	4.75	3.2	test	Weld seams	123	800	67	93
(0,0,0)	7	3.2	superfast	Weld seams	121	740	124	276
(0,0,0)	7	3.2	fast	Weld seams	122	671	182	292
(0,0,0)	7	3.2	medium	Weld seams	123	678	249	401
(0,0,0)	7	3.2	slow	Weld seams	120	638	413	550

Pa) and Case 3: the analysis of only considering time-varying internal pressure alone where the temperature is maintained in normal ambient temperature (20 °C).

In terms of the stress field, the element proportions in the different distribution intervals of the mises stresses on the membrane surface during fire are counted in Fig. 17. Overall, the stress variation trend in Case 1 is approximately similar to the trends in the sum of Case 2 and Case 3. The membrane surface failure should be attributed to the coevolutionary results of the stress field on the membrane surface and the degraded material properties at elevated temperatures. Surprisingly, the results in Case 2 show that the membrane surface almost does not ocurr the stress redistribution for the first 50 s. In other words, high temperature below a certain level do not have a significant impact on the stress on the membrane surface for the membrane structures in some particularly hot areas. Meanwhile, when the temperature of the membrane surface continues to rise, the variation occurrs only in a small distribution interval (0-1 MPa). The results in Case 3 suggest that when the internal pressure is maintained at a high level (around 800 Pa), the increase of membrane surface temperature has little repercussion on the stress distribution. Of course, this may also be because the number of stress division intervals is so small that the stress redistribution is not be reflected in the data.

For the failure element at weld seams in the simulation, Fig. 18 shows the time history of temperature and internal pressure acting on the element, and Fig. 19 compares the changes of failure parameters of the element in three cases above mentioned. It can be found that in the first 100 s, the failure parameters are very small and the corresponding temperatures are less than 100 ℃. However, the failure at weld seams occurs rapidly in a short time after the temperature reaches around 100 ℃. The statistical information of the failure element is summarised in Table 2, and it can be seen from the data that without the help of high temperature, high pressure is difficult to damage the membrane surface, that is to say, the temperature factor plays a dominant role in membrane surface failure under fire compared to the internal pressure factor.

4. Parametric studies

To more completely elaborate the membrane surface failure under fire, 10 groups of additional working conditions where the variables involved are fire source locations, fire source powers, fire source growth types and so on, are conducted. The coordinate system has the center of the structure as the origin and the long axis as the X-axis. Details of all working conditions and corresponding simulation results are presented in Table 3.

Comparing the simulation results, it is illustrated that the failure time is positively correlated with the height of the membrane surface above the fire source and negatively correlated with the maximum fire power and the growth type. The failure time of the membrane surface obtained by the thermal-mechanical coupling method is obviously shorter than that by the previous method of only temperature factor. Furthermore, eight groups of membrane surface failure in ten groups of working conditions occur at the weld seams, which indicates that the weld seams are the weak part of the air-supported membrane structure subjected to fire.

Fig. 20 provides critial failure temperature and critical failure internal pressure of the failure element in various conditions. It can be observed that the critical temperature of initial failure at weld seams (119–123 ℃) is smaller than the critical failure temperature of UTS of the weld seams (130 ℃) obtained by Eq. (17) and the critical temperature of the membranes initial failure is approximately 136 ℃, which is lower than the critical temperature for UTS of the membranes at 250 ℃ obtained by Eq. (7). In the thermal-mechanical coupling analysis, the critical failure temperature of the membrane surface failure is much lower than the burn-through temperature of the membrane materials (257–437.6 ℃) [3,4]. What's more, the amount of internal pressure (ranging from 200 pa to 800 pa) is not significantly affect the critical temperature for membrane surface failure. The reason could be that the internal pressure has little effect on the force of the weld seams in the structural span direction compared with the other weld seams [59]. This also means that simply relieving the fire-induced high pressure through some structural or operational measure may not improve obviously the membrane failure threshold.

Based on the parametric analysis results, if the temperature continues to be the only index to evaluate membrane surface failure in the air-supported membrane structure under fire, the common reference failure temperature, e.g., burn-through temperature, should be reduced according to UTSs of membrane materials. Due to the feature that the membrane surface easily failed for the air-supported membrane structure under fire, it is not reasonable to determine the ultimate state of fire resistance of structure simply from the point of view of structural damage in order to maximize the use function of the building. The definition of the fire resistance rating should be based on the safety of personnel [60].

5. Conclusions and prospects

Based on the fire test case of full-scale air-supported membrane structure by HIT team, the membrane surface failure considering weld seams is analyzed, and the relevant conclusions and prospects are as follows:

(1) In the case of building fire, it is a race against time for personnel to escape. This paper provides a more accurate method for predicting membrane surface failure. The proposed general constitutive models of membranes and weld seams can be used to approximate the properties at any high temperature according to the tensile properties at room temperature. The established simulation methods to analyze the membrane surface failure from the perspective of thermal-mechanical coupling is effective and applicable. This study enriches the means of fire resistance analysis for membrane structures, but it also needs to be examined and improved.

(2) In particular both Hashin's criterion and Tsai-hill's criterion can realize the evaluation of membrane surface failure despite the complexity of membrane surface stress state under fire. The weld seams are the weak parts. The increase of internal pressure caused by the fire did not significantly lower the critical failure temperature of the weld seam. The time and position of membrane surface failure should be the coevolutionary results of membrane surface stress field and the time-varying strength of membrane materials. It cannot be simply considered that the failure must initially appear in the place with the maximum temperature on the membrane surface. If the temperature still are used to analyze the membrane surface failure, the reference temperature index should be discounted according to the critical failure temperature of strengths of the membranes and the weld seams respectively.

(3) The membrane surface is easy to fail for air-supported membrane structures under fire. The holes developed by the membrane surface failure will decrease the internal pressure, which accelerates the deflation and collapse of the structure. However, the membrane surface failure also has several benefits, such as smoke and toxic gas emissions and lowering the internal air temperature. Therefore, on the basis of the present work, it is worthwhile to continue to carry out and study more complex safety evacuation problems under fire.

(4) The air-supported membrane structure is also the wind-sensitive structure. The present study is valuable in coupled analysis of fire and wind disasters in the future.

CRediT authorship contribution statement

Yaning Zhang: Writing – review & editing, Writing – original draft, Software, Data curation, Conceptualization. **Ying Sun:** Writing – review & editing, Supervision, Project administration, Funding acquisition. **Qiming Zhu:** . **Zhenggang Cao:** Project administration, Investigation, Funding acquisition. **Yang Yu:** Software.

Declaration of competing interest

The authors declare that they have no conflict of interest.

Data availability

No data was used for the research described in the article.

Acknowledgment

The present work was conducted through the financial support of the National Natural Science Foundations of China (Project designation: 52178132 and Project designation: 52278167).

References

[1] P.W. Kneen, Prestressed membrane structures—the ultimate thin-walled structure, Thin Walled Struct. 9 (1-4) (1990) 135–149.
[2] T. Lan, Achievements and prospects of China's spatial structure in the past 70 years, Build. Struct. 49 (19) (2019) 5–10.
[3] G. Chai, G. Zhu, J. Zhou, et al., Experimental study on burn through properties of PVC membrane room under fire, Case Stud. Therm. Eng. 26 (2021) 101212.
[4] Y. Zhang, G. Zhu, H. Yang, Experimental research on combustion characteristics of air-supported membrane materials, Procedia Eng. 52 (2013) 624–629.
[5] Ma J.D.. Experimental Study on Mechanical Properties of Building Membrane at High Temperature. Harbin: Harbin Institute of Technology.
[6] Y. Yu, Z. Cao, Y. Sun, Mechanical properties of four types of PVC-coated woven fabrics at high-temperature and after exposure to high-temperature, Structures 33 (1) (2021) 830–840.
[7] S.D. Xue, F. Yan, G.J. Sun, Mechanical properties of coated fabric membranes at high temperature, J. Eng. Fiber Fabr. 17 (2022) 1–12.
[8] J.S. Hopkinson, Fire tests on an air supported structure, Fire Saf. Sci. 955 (1972) 1.
[9] R. Custer, Test burn and failure mode analysis of an air-supported structure, Fire Technol. 8 (1) (1972) 19–23.
[10] SP Swedish Nationgal Testing Institute, Full-Scale Fire Test on Composite Membranes for Textile structure, SP Swedish National Testing Institute, Boras, 1998.
[11] Y. Yu, Y. Sun, Z. Cao, Fire test study of full-scale air-supported membrane structure in large space, Thin Walled Struct. 190 (2023) 111039.
[12] Y.K. Shen, Z.P. Wang, C.B. Peng, et al., Fire temperature field and smoke distribution of rectangular gas-filled diaphragm structure, Ind. Build. 44 (9) (2014) 78–82.
[13] S.L. Yi, B. Zeng, Fire temperature field characteristics of inflatable diaphragm structure, Fire Sci. Technol. 35 (11) (2016) 1507–1510.
[14] H. Zhang, Simulation of Fire Temperature Field of Large-Space Gas-Borne Membrane Structure, Harbin Institute of Technology, Harbin, 2020.
[15] J.Y. Wu, G.J. Sun, S.D. Xue, Numerical simulation of fire in rectangular gas-bearing membrane Structures based on FLUENT, in: Proceedings of the 17th Academic Conference on Spatial Structures, 2018.
[16] Z. Cheng, S.D. Xue, X.Y. Li, Research progress and prospect of fire resistance of gas supported membrane structure coal shed, Build. Struct. 51 (S1) (2019) 583–587.
[17] Y. Yu, Z. Cao, Y. Sun, et al., Simulation of internal pressure FDS in gas-supported membrane structures under fire conditions, J. Northeast. Univ. 43 (08) (2022) 1176–1182 (Natural Science Edition).
[18] Y. Zhou, Z.E. Sun, C. Qian, Structural properties and application status of building membrane and gas membrane, New Build. Mater. 43 (8) (2016) 96–99.
[19] F. Guo, Combustion Characteristics of Fabric Membrane and Overall Stability Analysis of Inflatable Membrane Structure in Case of Fire, China University of Mining and Technology, Xuzhou, 2016.
[20] J. Zhou, G. Zhu, Y. Gao, et al., Numerical study on the effects of opening form on the deflation for an air-supported membrane structure, Case Stud. Therm. Eng. 13 (2019) 100404.
[21] G. Chai, G. Zhu, J. Zhou, et al., Fire risk analysis of air-supported membrane structure coal storage shed, in: Proceedings of the 2019 9th International Conference on Fire Science and Fire Protection Engineering (ICFSFPE), IEEE, 2019, pp. 1–9.
[22] J.J. Zhou, Study on Fire Reaction of PVC Membrane and Overall Stability of Gas-Bearing Membrane Structure Under Fire, China University of Mining and Technology, Xuzhou, 2020.
[23] T.G. Xie, S.C. Lu, YL. Huang, Fire protection design of gas-bearing membrane roof, Fire Sci. Technol. 42 (01) (2023), 75-78+93.
[24] Z.P. Wang, Fire Resistance Analysis of Rectangular Inflatable Membrane Structure, Xi 'an University of Architecture and Technology, 2014.
[25] F. Yan, G.J. Sun, S.D. Xue, Study on membrane damage and collapse of air-supported structures under fire condition, Fire 5 (5) (2022) 162, 5050162.
[26] J.W. Chen, S.X. Wu, B. Zhao, et al., Temperature effect on tensile mechanical properties of braided composite membranes, J. Southeast Univ. 50 (2) (2020) 251–259. Natural Science Edition.
[27] Y.Y. Zhang, Q.L. Zhang, H.L. Lv, et al., Influence of environment on mechanical properties of PVC membrane material, in: Proceedings of the 14th Academic Conference on Spatial Structure. Fuzhou: Spatial Structure Committee of Bridge and Structural Engineering Branch, Chinese Society of Civil Engineering, 2012, pp. 316–321.
[28] Y.Y. Zhang, Q.L. Zhang, H.L. Lv, Mechanical properties of polyvinylchloride-coated fabrics processed with Precontraint® technology, J. Reinf. Plast. Compos. 31 (23) (2012) 1670–1684.
[29] A. Ambroziak, P. Kłosowski, Influence of thermal effects on mechanical properties of PVDF-coated fabric, J. Reinf. Plast. Compos. 33 (7) (2014) 663–673.
[30] F.L. Zhao, B.J. Chen, Y.L. He, et al., Experimental study on high temperature mechanical properties of PVDF coated fabric membranes and joints, Spat. Struct. (3) (2014) 42–47.
[31] G.J. Sun, L. Li, S.D. Xue, et al., Mechanical properties of polyester-coated fabric membrane material subjected to uniaxial loading at elevated temperatures, J. Mater. Civ. Eng. 33 (7) (2021) 04021169.
[32] V. Kodur, M. Dwaikat, R. Fike, High-temperature properties of steel for fire resistance modeling of structures, J. Mater. Civ. Eng. 22 (5) (2010) 423–434.
[33] R.B. Hetnarski, M.R. Eslami, G.M.L. Gladwell. Thermal stresses: advanced theory and applications[M], Springer, Berlin, 2009.
[34] G.L. Shen, G.K. Hu, Mechanics of Composites, Tsinghua University Press, 2006.
[35] I.N. Shardakov, A.N. Trufanov, Identification of the temperature dependence of the thermal expansion coefficient of polymers, Polymers 13 (18) (2021) 3035 (Basel).
[36] Association T.. European design guide for tensile surface structures. 2004.
[37] S.D. Xue, F. Yan, G.J. Sun, Deflation and collapse of air-supported membrane structures, Thin Walled Struct. 169 (2021) 108338.
[38] R. Pyke, The use of linear elastic and piecewise linear models in finite element analyses. Geomechanical Modelling in Engineering Practice, Routledge, 2021, pp. 167–187.
[39] S.H. Chen, Study on Tensile Properties of Woven Building Membrane Materials: from Uniaxial, Biaxial to Multi-Axial, Textile College, Donghua University, Shanghai, 2008.
[40] H.L. Yi, X. Ding, S.H. Chen, PES/PVC membrane material anisotropy of tensile properties and failure criteria [J], J. Compos. Mater. 22 (06) (2005) 98–102.
[41] J. Xu, Y. Zhang, Q. Yu, et al., Analysis and design of fabric membrane structures: a systematic review on material and structural performance, Thin Walled Struct. 170 (2022) 108619.
[42] R.A. Toupin, Saint-Venant's principle, Arch. Ration. Mech. Anal. 18 (1965) 83–96.
[43] Y. Yu, Study on Fire Resistance Test and Numerical Simulation of Air-Supported Membrane Structure, Harbin Institute of Technology, Harbin, 2022.
[44] J. Ye, Y. Wang, Z. Li, et al., Failure analysis of fiber-reinforced composites subjected to coupled thermo-mechanical loading, Compos. Struct. 235 (2020) 111756.
[45] H. Li, W. Lu, H. Zhao, Thermal-mechanical coupling of pressure vessel by finite element method, J. Chongqing Univ. Technol. 30 (9) (2016) 43–48 (Natural Science).
[46] Y. Li, X.Z. Lu, P.Q. Ren, et al., An equivalent time method for simulating continuous fire collapse, Build. Sci. 29 (9) (2013) 8–12.
[47] Hibbitt, Karlsson, Sorensen. ABAQUS analysis user's manual (Version 6.8). Pawtucket: Rhode Island, 2008.
[48] J.A. Milke, Analytical methods to evaluate fire resistance of structural members, J. Struct. Eng. 125 (10) (1999) 1179–1187.
[49] Y. Yang, S. Qian, J. Gong, et al., Design method for precise-forming of air-supported structures considering weld seams, Thin Walled Struct. 145 (2019) 106397.
[50] C. Williams,1980. Form finding and cutting patterns for air-supported structures. in Air-supported structures: the state of the art. Institution of Structural Engineers, London, pp. 99-120.
[51] Y.Y. Zhang, Q.L. Zhang, Mechanical Properties of Coated Fabric Building Membrane Materials, China University of Mining and Technology Press, 2013.
[52] J. Song, Research on Bursting Resistance of Coated Fabric Membrane, China University of Mining and Technology, 2019.
[53] Y. Cai, X. An, Q. Zou, et al., Damage behaviors of plain-woven fiber reinforced composites with different orientations: from mesoscopic evolution to macroscopic performance prediction, Compos. Struct. 324 (2023) 117569.
[54] Hietaniemi J., Hostikka S., Vaari J., et al. FDS simulation of fire spread – comparison of model results with experimental data. 2004.
[55] A.A. Khan, A. Usmani, J.L. Torero, Evolution of fire models for estimating structural fire-resistance, Fire Saf. J. 124 (2021) 103367.
[56] Technical specification for fire prevention of Building Steel structures [S], 2024.

[57] J. Duan, D. Shi, J. Wang, et al., Study on response behavior of steel structure under fire environment by FDS-ABAQUS thermal coupling method, Eng. Mech. 34 (2) (2017) 197–206.
[58] J. Zhang, Research on Forming and Mechanical Properties of Prefabricated Inflatable membrane Structure, Harbin Institute of Technology, 2022.
[59] X. Li, Z. Zhang, S. Xue, et al., Experimental and simulation analysis of the initial shape of a large-span air-supported membrane structure, Thin Walled Struct. 178 (2022) 109491.
[60] W. Ren, J. Zhao, Y. Hua, Study of fire resistance of building structures and evacuation under fire, J. Disaster Prev. Mitig. Eng. 38 (01) (2018) 168–177.